A&A 377, 113–122 (2001)
DOI: 10.1051/0004-6361:20011031

Astronomy & Astrophysics

Spectroscopic nonadiabatic observables in β Cephei models

H. Cugier and J. Daszyńska

Astronomical Institute of the Wrocław University, ul. Kopernika 11, 51-622 Wrocław, Poland

Received 4 May 2001 / Accepted 11 July 2001

Abstract. We calculate time sequences of Si III 455.26 nm line profiles for 10 $M_\odot$ models using results of the linear nonadiabatic calculations of Dziembowski & Pamyatnykh (1993) for oscillations of β Cephei stars. The spectroscopic observables are amplitude ratios and phase differences for various oscillating parameters derived from line profiles. We search theoretical diagrams involving these observables for unstable modes with low harmonic degrees ($\ell = 0$, 1 and 2) and azimuthal orders of $m = -\ell, \ldots, +\ell$. We show that all unstable modes are grouped in domains assigned by different ℓ and m-values. In almost all studied diagrams, the retrograde ($m > 0$), prograde ($m < 0$) and zonal ($m = 0$) modes are well separated from each other. The clearest separation of the domains occurs for the m-values in the diagram making use of the first and second moments of line profiles. Neither the inclination angle i or the amplitude of the stellar radius variation ϵ change this conclusion. The diagram is however sensitive to the equatorial velocity v_e of the star. The method of determination of m is valid and efficient for the equatorial rotational velocity $20 < v_e < 50$ km s^{-1}. The observables studied here are usually by-products of periodogram analyses of time series of observed characteristics of line profiles. Our results point to the significance of such data for asteroseismology in addition to measurements of oscillation frequencies and photometric nonadiabatic observables.

Key words. stars: variables: general – stars: oscillation – stars: early-type

1. Introduction

After identification of their driving mechanism, β Cephei stars became attractive targets for asteroseismology, cf. Dziembowski & Pamyatnykh (1993) and Gautschy & Saio (1993). The crucial step for this goal is identification of oscillation modes, i.e., determination of the spherical harmonic degree, ℓ, the azimuthal order, m, and the radial order, n, for observed modes. Unfortunately, the frequency spectra of β Cephei stars are scarce (cf. Sterken & Jerzykiewicz 1993), which makes the task of mode identification difficult. Having linear nonadiabatic models of stellar oscillations Cugier et al. (1994) developed methods of determination of the ℓ-value employing data on light, colour, radial velocity amplitudes and phases. They found that all unstable modes are grouped in well-separated domains assigned by different ℓ-values. In the case of radial pulsations n-values can also be found from the photometric nonadiabatic observables. However, the m-values cannot be inferred from photometry. Determination of m is possible from an analysis of spectral line profile changes, as first noted by Ledoux (1951). Balona (1986a,b, 1987) proposed an algorithmic method to identify the oscillation modes based on the first few moments of line profiles. This method was first used by Aerts et al. (1992) to analysis of the β Cephei star δ Ceti.

In this paper we investigate how the above mentioned nonadiabatic models of stellar oscillations can be used to the analysis of spectroscopic data. For this purpose we calculated the amplitude ratios and the phase differences – the nonadiabatic observables – of various measured parameters from time series of theoretical line profiles corresponding to β Cephei models. We discuss how such data may be used to infer the n, ℓ and m-values of the mode.

The plan of the paper is as follows. First, in Sect. 2, we describe the method of calculation of observable parameters. The results for unstable modes with $\ell = 0$, 1, 2 and $m = -\ell, \ldots, +\ell$ for the Main Sequence stellar models with the mass equal to 10 $M_\odot$ are presented in Sect. 3. Using plots of different observables we look for the best way of determining the ℓ, m and n-values from spectroscopic and photometric data. In Sect. 4 we discuss the general significance of the nonadiabatic observables for β Cephei star asteroseismology.

2. Model calculations

In the present work we rely on results of the oscillation survey for Main Sequence stars in the mass range from 7 to 16 $M_\odot$ made by Dziembowski & Pamyatnykh (1993). Photometric properties of the unstable models of β Cephei

Send offprint requests to: H. Cugier,
e-mail: cugier@astro.uni.wroc.pl

stars are discussed by Cugier et al. (1994). Here we recall basic definitions suitable for modelling line profiles.

As usually the harmonic time dependence, $\exp(\mathrm{i}\omega_{n\ell m}t)$, and spherical harmonic horizontal dependence are assumed for the first order perturbed quantities, viz.

$$Y_\ell^m(\theta',\phi') \equiv N_\ell^m P_\ell^{|m|}(\cos\theta')\mathrm{e}^{\mathrm{i}m\phi'}, \quad (1)$$

where $P_\ell^m(\cos\theta')$ is the associated Legendre function and

$$N_\ell^m = \sqrt{\frac{(\ell-|m|)!}{(\ell+|m|)!}\frac{2\ell+1}{4\pi}} \quad (2)$$

is the normalization factor. The spherical harmonics form the orthonormal base, therefore we can use the following relation between the spherical harmonics expressed in (r',θ',ϕ') and (r,θ,ϕ) coordinate systems:

$$Y_\ell^m(\theta',\phi') = \sum_{k=-\ell}^{\ell} d_{\ell mk}(i) Y_\ell^k(\theta,\phi), \quad (3)$$

where i is the angle between polar axes of the both coordinate systems,

$$d_{\ell mk}(i) \equiv$$

$$\sum_r (-1)^{k-m-r} \frac{[(\ell+m)!(\ell-m)!(\ell+k)!(\ell-k)!]^{1/2}}{r!(\ell+m-r)!(\ell-k-r)!(k-m+r)!}$$

$$\times \cos(i/2)^{2\ell+m-k-2r} \sin(i/2)^{k-m+2r}$$

and

$$r \geq 0, r \geq m-k, r \leq \ell-k, r \leq \ell+m.$$

The real part of the eigenfrequency, $\omega_{n\ell m} = \omega^R_{n\ell m} + \mathrm{i}\omega^I_{n\ell m}$, gives the oscillation period

$$\Pi = 2\pi / Re(\omega_{n\ell m}) \quad (4)$$

and the nondimensional frequency

$$\sigma_{n\ell m} = Re(\omega_{n\ell m})/(4\pi G <\rho>)^{1/2}, \quad (5)$$

where $<\rho>$ is the mean density of the star and G– gravitational constant.

In this paper we use the zero-rotation approach. It does not mean that the star does not rotate, but rather that we are using the zero-rotation approximation to describe the oscillation modes as in Dziembowski & Pamyatnykh (1993). The important property of the eigenfunctions corresponding to β Cep stars is that they are nearly constant in the atmosphere, cf. Cugier et al. (1994). This fact justifies use of static atmospheric models for evaluating line profile changes, provided that the effects of oscillations are taken into account in the effective temperature and gravity, viz.

$$\begin{aligned} T_{\rm eff} &= T^0_{\rm eff} + \delta T_{\rm eff} = T^0_{\rm eff} + \varepsilon T^0_{\rm eff} \frac{1}{4} f_{\rm T} \\ &\times Re\Big\{ \exp\left(\mathrm{i}\left[(\omega_{n\ell m} - m\Omega)t + \psi_{\rm T}\right]\right) \\ &\times \sum_{k=-\ell}^{\ell} d_{\ell mk}(i) Y_\ell^k(\theta,\phi) \Big\} \end{aligned} \quad (6)$$

and

$$\begin{aligned} g &= g^0 + \delta g = g^0 - \varepsilon g^0 (3\sigma^2_{n\ell m} + 2) \\ &\times Re\Big\{ \exp(\mathrm{i}(\omega_{n\ell m} - m\Omega)t) \sum_{k=-\ell}^{\ell} d_{\ell mk}(i) Y_\ell^k(\theta,\phi) \Big\}, \end{aligned} \quad (7)$$

where ε is the amplitude of the stellar radius variations, Ω is the angular velocity of stellar rotation, i is the angle between the rotation axis and direction to the observer. The subscript zero denotes the stellar equilibrium model. Both $f_{\rm T}$ and $\psi_{\rm T}$ are evaluated from the complex f-eigenfunction describing surface variations of the local luminosity.

As pointed out by Dziembowski (2001, private communication) Cugier's et al. (1994) formula describing the local changes of gravity $\delta g/g^0$ due to pulsation should be modified to be more consistent with the relative pressure perturbation near the outer boundary condition. We therefore clarify here this point in some detail, following W. Dziembowski. It is well-known that the plane-parallel static models of atmospheres obey the relation $P = \tilde{m}g^0$, where P is the total pressure and $\tilde{m}$ is the mass over the unit area. This means that the change of gravity results in $\Delta P/P = \Delta g^0/g^0$ at any mass depth $\tilde{m}$. Δ is not the Lagrangian variation; the later is denoted by δ. For the gravity variations we may adopt

$$\frac{\Delta g^0}{g^0} = \frac{\delta g}{g^0} = -2\frac{\delta r}{R} - \frac{(\omega^R_{n\ell m})^2 R}{g^0}\frac{\delta r}{R} = -(2+3\sigma^2_{n\ell m})\frac{\delta r}{R}, \quad (8)$$

where R means the equilibrium stellar radius. The Lagrangian variation of the pressure is given by

$$\frac{\delta P}{P} = \frac{\delta g}{g^0} + \frac{\delta\tilde{m}}{\tilde{m}} = \frac{\delta g}{g^0} - \frac{\delta S}{S},$$

where

$$\frac{\delta S}{S} = 2\frac{\delta r}{R} + \frac{\cos\theta}{\sin\theta}\delta\theta + \frac{\partial\delta\theta}{\partial\theta} + \frac{\partial\delta\phi}{\partial\phi}$$

is the change of the surface of the fluid element. Substituting expressions for $\delta\theta$ and $\delta\phi$ given e.g. by Aerts et al. (1992) and taking into account that the spherical harmonics satisfy the equation

$$\left[(1-x^2)\frac{\partial^2}{\partial x^2} - 2x\frac{\partial}{\partial x} - \frac{m^2}{1-x^2} + \ell(\ell+1)\right] Y_\ell^m(\theta,\phi) = 0$$

$(x = \cos\theta)$ one can obtain

$$\frac{\delta S}{S} = \left(2 - \frac{\ell(\ell+1)}{3\sigma^2_{n\ell m}}\right)\frac{\delta r}{R}.$$

We therefore have

$$\frac{\delta P}{P} = -\left(3\sigma^2_{n\ell m} + 4 - \frac{l(l+1)}{3\sigma^2_{n\ell m}}\right)\frac{\delta r}{R} \quad (9)$$

in agreement with the pressure eigenfunction p near the outer boundary condition given by Eq. (7) of Cugier et al. (1994). In practice, the above mentioned correction for the surface gravity changes will be very small. For the lowest

order p-modes $\sigma = 2$, thus $\delta g/g^0 = 14\delta r/R$ instead of $\delta g/g^0 = 16\delta r/R$. Note that $\delta r/R$ is of the order of 0.01 for Main-Sequence stars. The difference decreases with radial overtone n and ℓ.

In summary, at a given pulsation phase the surface layers of nonradially oscillating Main-Sequence stars can be described by the family of static models of atmospheres which obey the relation $P = \tilde{m}g$, where the effective gravity is equal to $g = g^0(1+\delta g/g^0)$. This approach can be used as long as the following conditions are valid: (i) the plane parallel structure of the atmosphere (low values of ℓ) and (ii) the depth independence of the relevant eigenfunctions are maintained. It should be noted that the diffusion approximation for radiative transfer was used for the evaluation of the eigenfunctions, but in a full nonadiabatic way. The use of the nonadiabatic values for f-eigenfunction is essential for a description of the effective temperature (cf. Cugier et al. 1994). In this paper we used Kurucz's (1996) line-blanketed models as the above mentioned family of static stellar atmospheres.

The monochromatic flux of radiation at wavelength λ can be expressed as

$$\mathcal{F}_\lambda = \int I_\lambda(r,\theta,\phi,\boldsymbol{o}\cdot\boldsymbol{n})\frac{\mathrm{d}S_z}{R^2}, \tag{10}$$

where $I_\lambda(r,\theta,\phi,\boldsymbol{o}\cdot\boldsymbol{n})$ is the specific intensity of radiation at (r,θ,ϕ)-point propagating in the observer's direction $\boldsymbol{o}$ and $\boldsymbol{n}$ is the normal vector to the surface element $\mathrm{d}\boldsymbol{S}$. The z-component of $\mathrm{d}\boldsymbol{S}$ (z-axis is directed towards the observer) is given by (cf. e.g., Heynderickx et al. 1994)

$$\begin{aligned}\mathrm{d}S_z \;=\; & \left[R\sin\theta\left(R\cos\theta + 2\cos\theta\delta r + \sin\theta\frac{\partial\delta r}{\partial\theta}\right)\right.\\ & +R^2(\cos^2\theta-\sin^2\theta)\delta\theta\\ & \left.+R^2\sin\theta\cos\theta\left(\frac{\partial\delta\theta}{\partial\theta}+\frac{\partial\delta\phi}{\partial\phi}\right)\right]\mathrm{d}\theta\mathrm{d}\phi,\end{aligned} \tag{11}$$

where

$$\delta r(r,\theta,\phi,t) = \varepsilon R y_{nlm}(R) \times \sum_{k=-\ell}^{\ell} d_{\ell mk}(i) Y_\ell^k(\theta,\phi)\cdot\exp(\mathrm{i}(\omega_{n\ell m}-m\Omega)t), \tag{12a}$$

$$\delta\theta(r,\theta,\phi,t) = \varepsilon R z_{nlm}(R) \times \sum_{k=-\ell}^{\ell} d_{\ell mk}(i)\frac{\partial Y_\ell^k(\theta,\phi)}{\partial\theta}\cdot\exp(\mathrm{i}(\omega_{n\ell m}-m\Omega)t), \tag{12b}$$

$$\delta\phi(r,\theta,\phi,t) = \varepsilon R z_{nlm}(R)\frac{1}{\sin^2\theta} \times \sum_{k=-\ell}^{\ell} d_{\ell mk}(i)\frac{\partial Y_\ell^k(\theta,\phi)}{\partial\phi}\cdot\exp(\mathrm{i}(\omega_{n\ell m}-m\Omega)t). \tag{12c}$$

The numerical integration of Eq. (10) requires evaluation of the specific intensities at many points distributed over stellar surface taking into account the Doppler effect due to the radial velocity of the surface elements relative to the observer. The velocity field of pulsating stars can be found calculating the time derivative of the fluid displacement $\boldsymbol{\xi}_{nlm}$. The radial component $v_{\mathrm{pul},r}$ formulated in the observer's frame (r,θ,ϕ) is

$$\begin{aligned}v_{\mathrm{pul,r}} \;=\; & \omega_{n\ell m}\varepsilon R\Big[y_{nlm}(R)\cos\theta\\ & \times\sum_{k=-\ell}^{\ell} d_{\ell mk}(i)N_\ell^k P_\ell^k(\theta)\sin((\omega^R_{n\ell m}-m\Omega)t+k\phi)\\ & -z_{nlm}(R)\sin\theta\sum_{k=-\ell}^{\ell} d_{\ell mk}(i)N_\ell^k\frac{\partial P_\ell^k(\theta)}{\partial\theta}\\ & \times\sin((\omega^R_{n\ell m}-m\Omega)t+k\phi)\Big].\end{aligned} \tag{13}$$

The functions $y_{nlm}(r)$ and $z_{nlm}(r)$ have the same meaning as in Cugier et al. (1994). The total radial velocity (as seen by a distant observer) due to pulsation and rotation is then

$$v_\mathrm{r} = v_{\mathrm{pul,r}} - v_\mathrm{e}\,\sin i\,\sin\theta\,\sin\phi, \tag{14}$$

where v_e represents the equatorial velocity of rotation. We assumed rigid rotation with v_e = const. during pulsation cycle. We also neglected poloidal and toroidal terms in the fluid displacement due to the Coriolis force. Test calculations show that this is acceptable for models presented here, because we limited ourselves to stars with the low rotational velocity ($v_\mathrm{e} \le 50\ \mathrm{km\,s^{-1}}$).

The opacity and emissivity of the stellar material, as seen by a stationary observer, become dependent on the angle between local velocity vector $\boldsymbol{v}$ and the direction to the observer $\boldsymbol{e}_z$. If the wavelength in the observer's frame is λ, then in the atom frame the wavelength at which a photon travelling in the direction $\boldsymbol{e}_z$ was emitted, or can be absorbed, is $\lambda' = \lambda - \lambda_0\boldsymbol{v}(-\boldsymbol{e}_z)/c = \lambda - \lambda_0 v_\mathrm{r}/c$. The formal solution of the transfer equation for the specific intensity allows a direct evaluation of the effects of velocity fields on profiles by accounting for the velocity induced shifts in the opacity and emissivity of the material. Some asymmetries in the line profiles calculated by integration of the local intensities over the stellar disk result even if there is no velocity gradient and the atmosphere is assumed to expand with constant velocity, cf. van Hoof & Deurinck (1952) and Duval & Karp (1978).

In this project, time series of line profiles are calculated for several models corresponding to β Cep stars and the numerical integration of Eq. (10) is time-consuming. In order to limit computing time it is convenient to introduce the normalised limb-darkening law $h_\lambda(\tilde{\mu})$ by the relation

$$I_\lambda(r,\theta,\phi,\tilde{\mu}=\boldsymbol{o}\cdot\boldsymbol{n}) = \frac{1}{2\pi}\mathcal{F}_\lambda(T_\mathrm{eff},g)h_\lambda(T_\mathrm{eff},g,\tilde{\mu}). \tag{15}$$

This formula gives the correct limb-darkening law as far as the flux and specific intensities are known. The common practice is to use the linear or quadratic form for $h_\lambda(T_\mathrm{eff},g,\tilde{\mu})$, cf. Wade & Rucinski (1985). The advantage is that only knowledge of $\mathcal{F}_\lambda$ and two limb-darkening coefficients for the local values of T_eff and g are necessary. (These coefficients are evaluated from $\mathcal{F}_\lambda(T_\mathrm{eff},g)$,

$I_\lambda(T_{\rm eff}, g, \tilde{\mu}=1.0)$ and $I_\lambda(T_{\rm eff}, g, \tilde{\mu}=0.1)$). Several tests show that for the spectral line investigated here we can make a further simplification introduced by Cugier (1993). This approach is based on the assumption that the local intensity of radiation can be expressed as

$$I_\lambda = I^0_\lambda + \delta I_\lambda = I^0_\lambda + \frac{1}{2\pi}(\delta\mathcal{F}_\lambda h^0_\lambda + \mathcal{F}^0_\lambda \delta h_\lambda)$$

and retaining only first order terms from the product of $I_\lambda {\rm d}S_z$ one can obtain

$$\mathcal{F}_\lambda = \frac{1}{2\pi}\int\int \mathcal{F}^0_\lambda\ G_\lambda(r,\theta,\phi)\ {\rm d}\theta\ {\rm d}\phi, \tag{16}$$

where the flux $\mathcal{F}^0_\lambda$ corresponds to the equilibrium model and

$$\begin{aligned} G_\lambda(r,\theta,\phi) \ =\ & h^0_\lambda \sin\theta\cos\theta + 2h^0_\lambda \sin\theta\cos\theta\frac{\delta r}{R} \\ & + h^0_\lambda \sin^2\theta \frac{\partial \delta r/R}{\partial\theta} + \frac{\partial h^0_\lambda}{\partial\mu}\sin^2\theta\cos\theta\frac{\partial\delta r/R}{\partial\theta} \\ & + h^0_\lambda \frac{\delta\mathcal{F}_\lambda}{\mathcal{F}^0_\lambda}\sin\theta\cos\theta + (\delta h^2_\lambda + \delta h^3_\lambda)\sin\theta\cos\theta \\ & + h^0_\lambda(\cos^2\theta - \sin^2\theta)\delta\theta \\ & + h^0_\lambda \sin\theta\cos\theta\left(\frac{\partial\delta\theta}{\partial\theta} + \frac{\partial\delta\phi}{\partial\phi}\right) \\ & - \frac{\partial h^0_\lambda}{\partial\mu}\sin^2\theta\cos\theta\delta\theta. \end{aligned} \tag{17}$$

The change of the local monochromatic flux can be expressed as

$$\begin{aligned} \frac{\delta\mathcal{F}_\lambda}{\mathcal{F}^0_\lambda} \ &=\ \frac{1}{\ln 10}\frac{\partial\log\mathcal{F}^0_\lambda}{\partial\log T^0_{\rm eff}}\frac{\delta T_{\rm eff}}{T^0_{\rm eff}} + \frac{1}{\ln 10}\frac{\partial\log\mathcal{F}^0_\lambda}{\partial\log g^0}\frac{\delta g}{g^0} \\ &=\ \alpha_{\rm T}(\lambda)\frac{\delta T_{\rm eff}}{T^0_{\rm eff}} + \alpha_g(\lambda)\frac{\delta g}{g^0}. \end{aligned} \tag{18}$$

In general, three effects may play a role on the limb−darkening changes

$$\delta h_\lambda = \delta h^1_\lambda + \delta h^2_\lambda + \delta h^3_\lambda. \tag{19}$$

The term δh^1_λ corresponds to the brightness effect due to local variation of the normal to the surface element, viz.

$$\delta h^1_\lambda = \frac{\partial h^0_\lambda}{\partial\mu}\left(\frac{1}{R}\frac{\partial\delta r}{\partial\theta} - \delta\theta\right)\sin\theta \tag{20a}$$

for small perturbations. The terms δh^2_λ and δh^3_λ describe sensitivity of the limb darkening effect on the temperature and gravity variations, respectively,

$$\delta h^2_\lambda = \frac{1}{\ln 10}\frac{\partial h^0_\lambda}{\partial\log T^0_{\rm eff}}\frac{\delta T_{\rm eff}}{T^0_{\rm eff}} \tag{20b}$$

and

$$\delta h^3_\lambda = \frac{1}{\ln 10}\frac{\partial h^0_\lambda}{\partial\log g^0}\frac{\delta g}{g^0}. \tag{20c}$$

Again, the integral in Eq. (16) can be evaluated by dividing the visible disk of the star into small elements, computing the radial velocity $v_{\rm r}$ at each point on the disk and adding up the appropriately Doppler shifted product of $\mathcal{F}^0_\lambda\ G_\lambda(r,\theta,\phi)$. Accuracy of the model calculations is satisfactory for continuum flux modelling even for a moderate number (about 6000) of surface elements distributed over the stellar disk, cf. Daszyńska & Cugier (1998). In the case of line profiles, using Eq. (16) instead of Eq. (10) leads to the maximum error of about 1.5%, which is acceptable for the purpose of this paper.

The computing code was further tested for each effect included in Eq. (17) by comparing them with the semi-analytical calculations when the Doppler effect is neglected. The assumption that the Doppler effect can be neglected is very well fulfilled for the continuum flux modelling. In this case all terms with $\delta\theta$ and $\delta\phi$ in Eq. (17) can be omitted because their total contribution to the integral over ϕ equals to zero.

Introducing the notations

$$b_\ell = \int_0^1 h^0(\tilde{\mu})\tilde{\mu}P_\ell(\tilde{\mu}){\rm d}\tilde{\mu}, \tag{21a}$$

$$T_1 = \frac{1}{4}f_{\rm T}\alpha_{\rm T}(\lambda)b^\lambda_\ell, \tag{21b}$$

$$T_2 = \frac{1}{4}f_{\rm T}\frac{1}{\ln 10}\frac{\partial b^\lambda_\ell}{\partial\log T_{\rm eff}}, \tag{21c}$$

$$T_3 = b^\lambda_\ell(2+\ell)(1-\ell), \tag{21d}$$

$$T_4 = -\Big(3\sigma^2_{n\ell m} + 2\Big)\alpha_g(\lambda)b^\lambda_\ell \tag{21e}$$

and

$$T_5 = -\Big(3\sigma^2_{n\ell m} + 2\Big)\frac{1}{\ln 10}\frac{\partial b^\lambda_\ell}{\partial\log g^0} \tag{21f}$$

we can write

$$\begin{aligned} \frac{\Delta\mathcal{F}_\lambda}{\mathcal{F}^0_\lambda} \ =\ & \varepsilon d_{\ell m0}N^0_\ell\big[(T_1+T_2)\cos\big(\big(\omega^R_{n\ell m} - m\Omega\big)t + \psi_{\rm T}\big) \\ & + (T_3+T_4+T_5)\cos\big(\omega^R_{n\ell m} - m\Omega\big)t\big]. \end{aligned} \tag{22}$$

In this formula, two terms T_1 and T_2 describe the temperature effects, whereas the influence of the gravity changes during pulsation cycle are contained in the T_4 and T_5 terms. The T_2 and T_5 terms reveal the sensitivity of the limb-darkening parameters to temperature and gravity variations, respectively. The term T_3 corresponds to the geometrical effects. This semi-analytical formula was already used by Cugier et al. (1994) for photometric nonadiabatic observables of β Cep stars, but now it is corrected for the surface gravity changes as described above. At a given phase of pulsation φ, the continuum flux level depends on the parameters of ε, l, m and i. The semi-analytical approach (Eq. (22)) reveals that these parameters occur as the product of $\varepsilon\, d_{\ell m0}(i)$. We would like to recall that ε is the amplitude of the stellar radius variation, whereas

$$d_{\ell m0}(i) = \sqrt{\frac{(\ell-|m|)!}{(\ell+|m|)!}}P^m_\ell(\cos i). \tag{23}$$

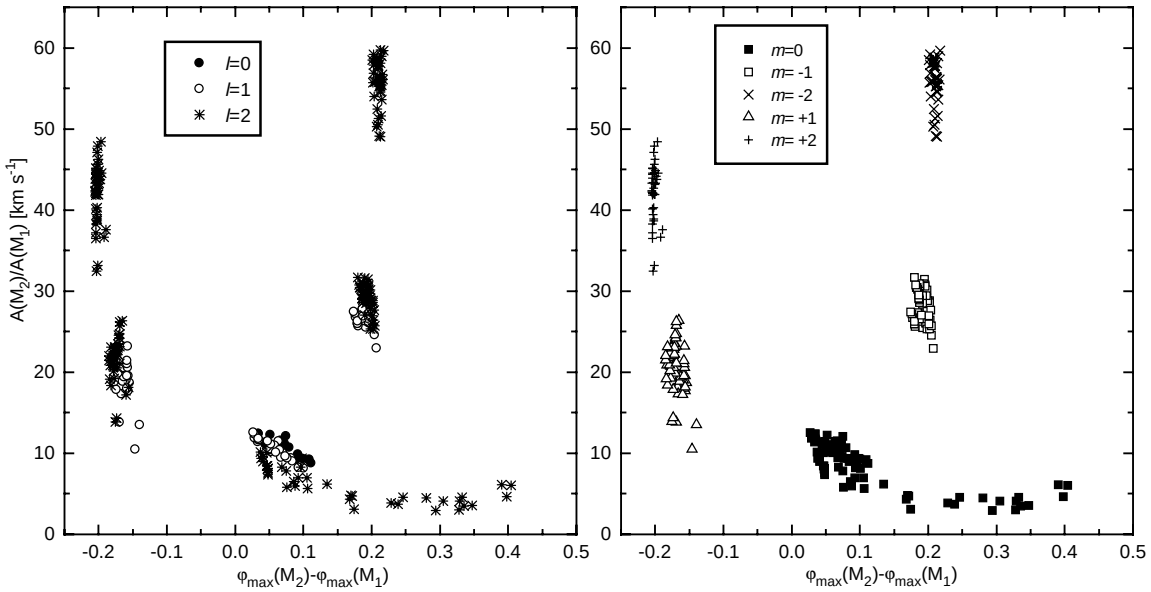

Fig. 1. The amplitude ratio vs. phase difference (in 2π radians) diagrams for the second (M_2) and first (M_1) moments of Si III 455.26 line profiles. The data shown by different symbols correspond to unstable modes ($\ell \leq 2$) for 10 $M_\odot$ Main-Sequence models. In the left panel the symbols used are assigned to ℓ-values, whereas the right panel shows the well−separated domains of modes with different m-values. The unstable modes were calculated by Dziembowski & Pamyatnykh (1993) for stellar models with the OPAL ($Z = 0.02$) opacities.

This means, for instance, that in the linear approximation the amplitude ratios of measurements in different photometric passbands depend neither on ε nor i. Furthermore, there are specific inclination angles i^* for which $d_{\ell m0}(i^*) = 0$ and no continuum flux variation can be seen despite the stellar radius variations with the amplitude of ε. The line profiles are also affected by the inclination angle, but even for $i = i^*$ the situation is different due to the Doppler effect. In particular, the line profiles show some changes during stellar pulsation although no continuum flux variability can be seen by a distant observer, cf. Daszyńska & Cugier (1998).

The above-given formulae self-consistently describe line profiles (Eqs. (16)–(17)) and continuum flux (Eq. (22)) variations during pulsation cycle for slowly rotating stars. As mentioned above this approach is adequate for modelling of Si III 455.26 nm line profiles of β Cep stars, but in general line profiles should be evaluated from Eq. (10), especially for lines when limb-darkening law differs markedly from the quadratic form (e.g., hydrogen lines of δ Scuti type stars or η Bootis). Discrepancies in both continuum and line profiles calculated by means of Eq. (16) instead of Eq. (10) increase with ℓ.

3. Identification of the spherical harmonic degree ℓ and the azimuthal order m for an observed mode

We investigate how the knowledge about nonadiabatic observables $f_{\rm T} = {\rm abs}[(f-2)/y]$ and $\psi_{\rm T} = \arg[(f-2)/y]$ can be used to determine the ℓ and m-values for β Cep stars from spectroscopy. For this purpose we calculated time series of line profiles for a star of 10 $M_\odot$ at selected epochs its Main Sequence evolution assuming $v_{\rm e} = 50$ km s^{-1}, $i = 60^{\rm o}$ and $\varepsilon = 0.015$. After normalization of the line profiles to the continuum level we measured various characteristics as a function of time and fitted a synthetic curve consisting of the six sine functions with the primary period and its first five harmonics. Then we constructed various diagrams making use of the amplitudes and phases for the primary period in order to search for the best discriminators of oscillation modes in β Cephei stars. We considered diagrams employing the following observables: $F_{\rm min}$ – residual intensity measured at the deepest point of the normalised line profiles, EW – equivalent width, $FWHM$ – full width at the half maximum, F_{λ_0} – line intensity at $\lambda_0 = 455.26$ nm, F_{λ_1} – line intensity at $\lambda_1 = \lambda_0 - 0.05$ nm, $V_{\rm min}$ – radial velocity corresponding to $F_{\rm min}$, $V_{\rm hm}$ – radial velocity corresponding to $FWHM$, M_0, M_1, M_2 and M_3 – zeroth and the first three moments of the line profile. The moments are defined as:

$$M_n = \int_{-a}^{a} (v - v_0)^n (1 - F(v)) {\rm d}v, \qquad (24)$$

where v_0 corresponds to λ_0, $a = 180$ km s^{-1} and $F(v)$ means the line profile at the velocity scale. By considering different diagrams we look for the most revealing parameters for mode identification. We found that the diagram of $A(M_2)/A(M_1)$ vs. $\varphi_{\rm max}(M_2) - \varphi_{\rm max}(M_1)$ is the best for m determination. On this diagram all modes are grouped in five domains (cf. Fig. 1). The left panel of Fig. 1 shows that modes are not separated between each other for different ℓ-values. The same is true for the radial number n. Only points corresponding to different m-values occur in

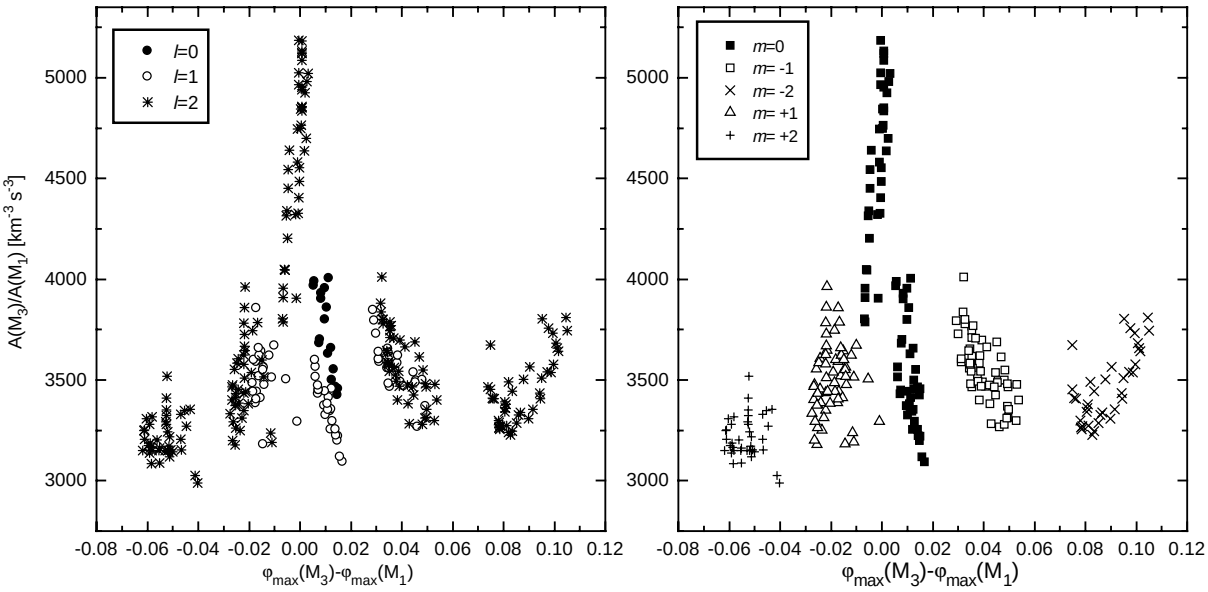

Fig. 2. As in Fig. 1, but for the third (M_3) and the first (M_1) moments of the line profiles. Again, on the right panel we can see the separation of the modes with regard to the azimuthal order m.

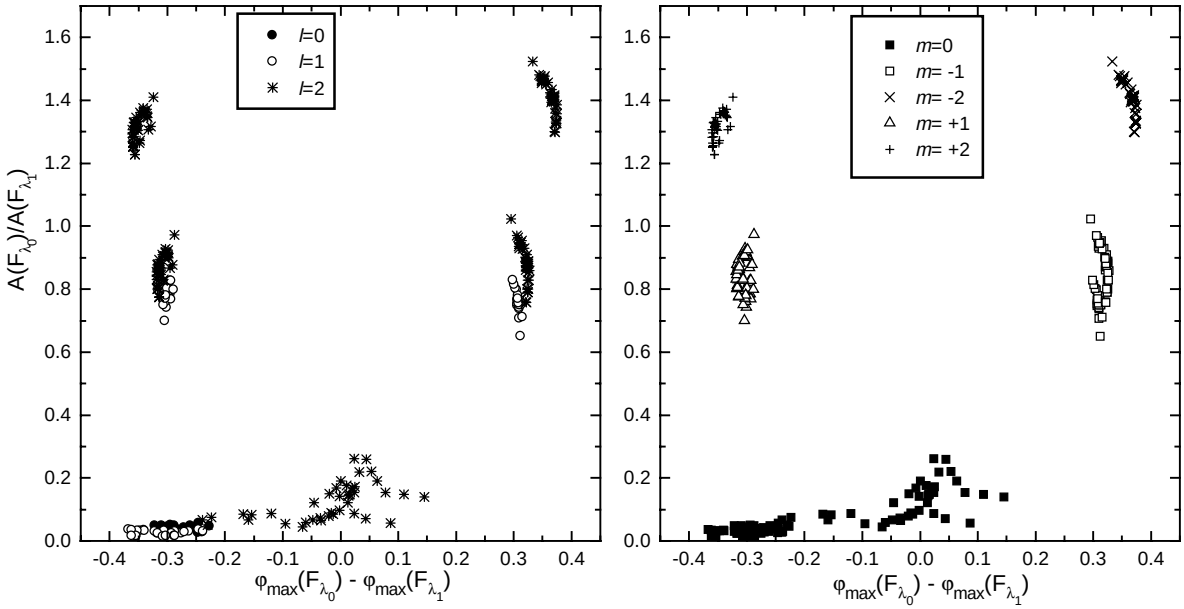

Fig. 3. As in Fig. 1, but for the monochromatic fluxes F_{λ_0} and F_{λ_1} measured at $\lambda_0 = 455.26$ nm and $\lambda_1 = 455.21$ nm.

the well separated domains, cf. right panel of Fig. 1. The M_3 and M_1 measurements (cf. Fig. 2) may also yield an unambiguous m-values as well as the pairs of $(F_{\lambda_0}, V_{\min})$, $(F_{\lambda_1}, V_{\min})$ and $(F_{\lambda_0}, F_{\lambda_1})$. The last diagram is shown in Fig. 3.

Now, we search for sensitivity of the results to the inclination angle i, amplitude of the stellar radius variation ε and stellar equatorial velocity $v_{\rm e}$. As an example we consider the stellar model of $\log T_{\rm eff} = 4.3693$ and $\log g = 3.914$ from the evolutionary track of 10 $M_\odot$ assuming several values for i (0, 10, ..., 90°), ε (0.0015, 0.01 and 0.02) and $v_{\rm e}$ (0, 10, 20, 30, and 50 km s^{-1}). Figures 4a and 5a indicate that different values of i do not change our conclusion about diagnostic values of the diagrams shown in the right panels of Figs. 1 and 2, respectively. The same is true for ε, cf. Figs. 4b and 5b. The fact that ε does not change the diagnostic value of these diagrams indicates that they can also be used in the case when a few modes with different amplitudes are excited simultaneously. The effect of $v_{\rm e}$ needs more caution, cf. Fig. 6. In the limit of $v_{\rm e} = 0$ all modes are located on a very small region. For $v_{\rm e} > 20$ km s^{-1} modes are clearly separated into domains

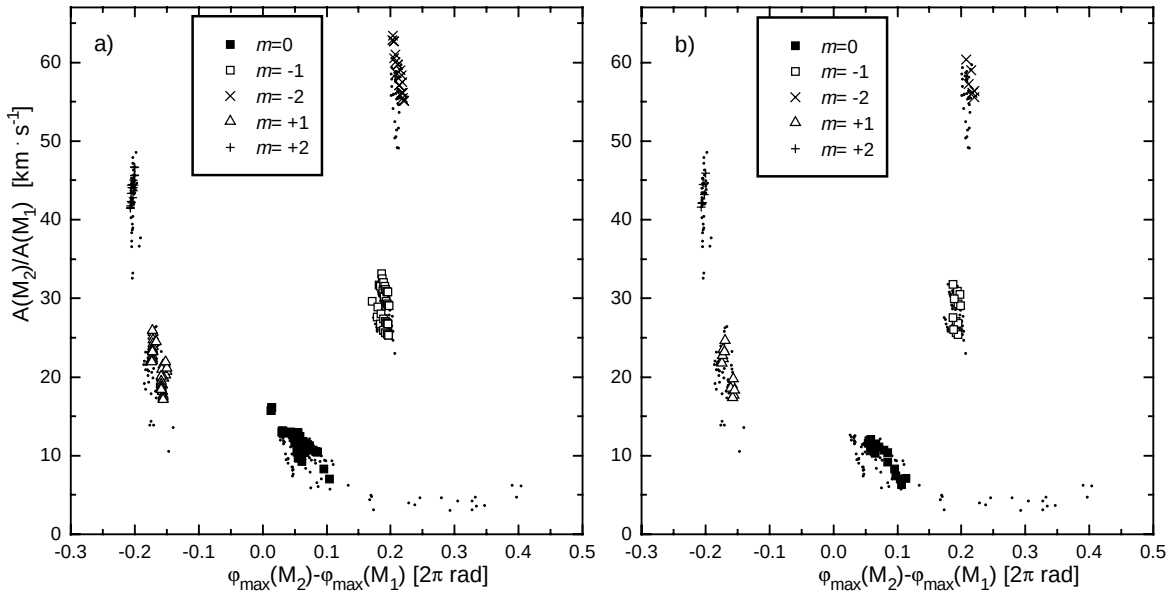

Fig. 4. The effect of the inclination angle i (panel **a)**) and the amplitude of the stellar radius variation ϵ (panel **b)**) for the model of $\log T_{\rm eff} = 4.3693$ and $\log g = 3.914$. The modes with different m-values are still located in the same domains as the modes in Fig. 1 marked here as small dots.

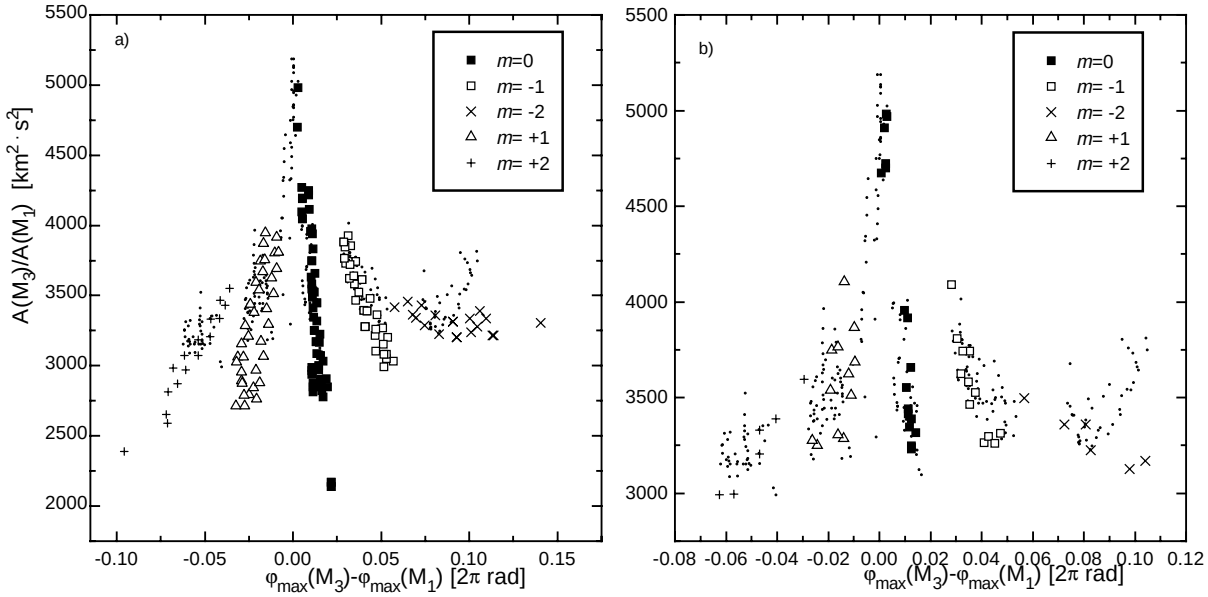

Fig. 5. As in Fig. 4, but for M_3 and M_1 measurements.

with different values of m. Similar behaviour can be seen for the M_3 and M_1 data, cf. Fig. 7.

On the diagrams above, the separation of different ℓ domains is not as clear as for m-values, but some diagrams investigated by us are still useful for identification of l, e.g., the $(FWHM, V_{\rm min})$-diagram. Much better constrains can, however, be obtained for the ℓ-values from the photometric nonadiabatic diagrams. As an example, Fig. 8 displays the diagram of (A_u/A_y) vs. $(\varphi_u - \varphi_y)$ for the Strömgren photometry. We can see that modes with different ℓ values are located in the well-separated domains. Additionally we show the effect of the microturbulent velocity (upper panel of Fig. 8) and metallicity in the stellar atmospheres (lower panel of Fig. 8).

4. Conclusions and discussion

In β Cephei stars the observed modes occur in narrow frequency ranges (cf. e.g., Sterken & Jerzykiewicz 1993) and unlike δ Scuti stars no more than one radial mode is observed. Nonradial modes may have very close frequencies owing to their mixed character,

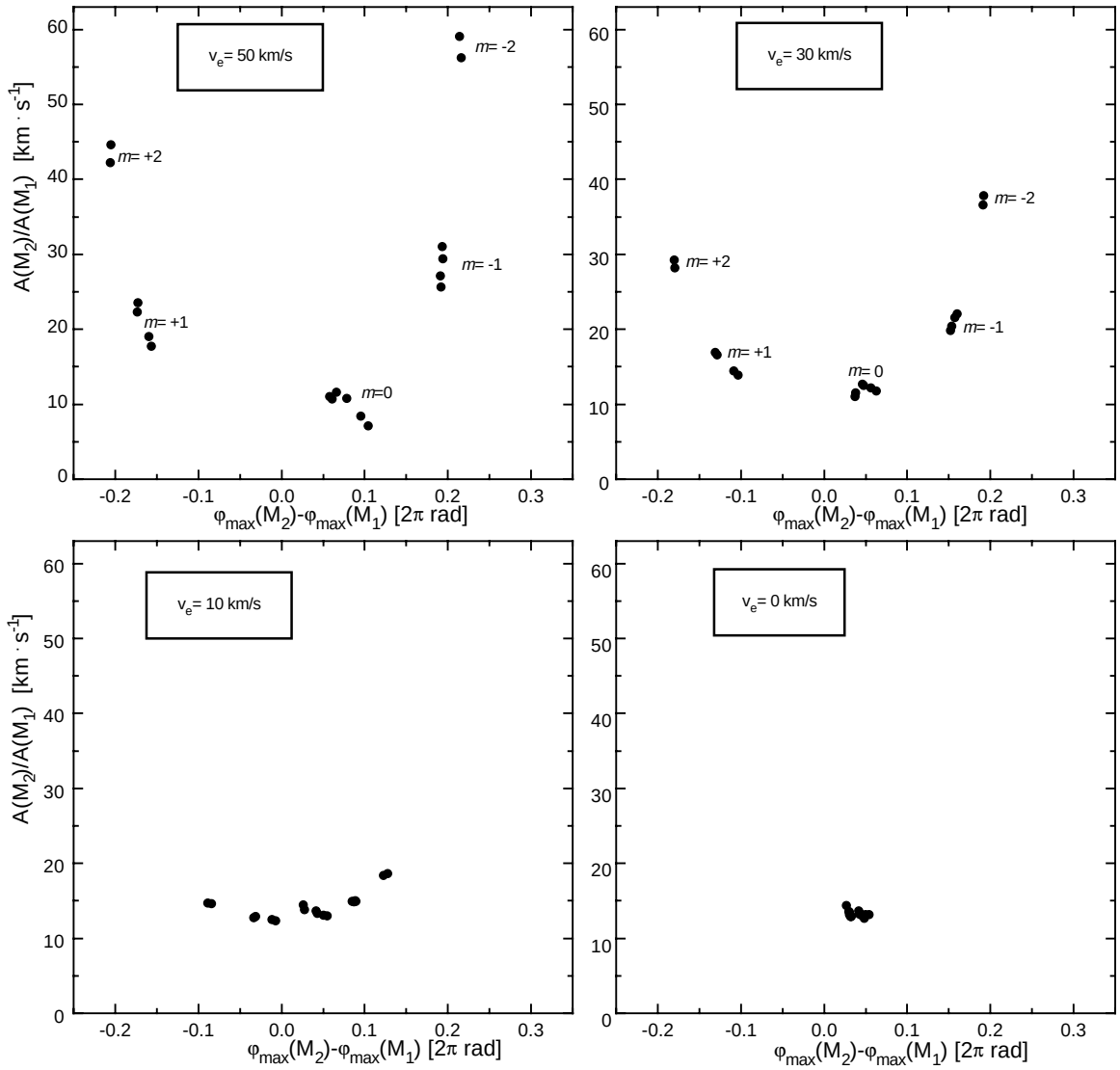

Fig. 6. The effect of the equatorial stellar rotation $v_{\rm e}$ on the diagram $A(M_2)/A(M_1)$ vs. $\varphi_{\rm max}(M_2) - \varphi_{\rm max}(M_1)$. The results are ploted in four panels for the same stellar model of $\log T_{\rm eff} = 4.3693$ and $\log g = 3.914$ but different values of $v_{\rm e}$, respectively. We can see that this diagram is very sensitive to the equatorial rotational velocity. The well-separated regions of modes with different m-values occur only for $v_{\rm e} \geq 20$ km s^{-1}.

cf. Dziembowski & Pamyatnykh (1993) and Gautschy & Saio (1993). Identification of the observed modes by other techniques is therefore an essential step for asteroseismology of these stars. It consists of determination of the spherical harmonic degree, ℓ, the azimuthal order, m, and the radial order, n. Cugier et al. (1994) focused on the ℓ-value determination from photometry and radial velocity measurements. They also demonstrate the usefulness of these observables for the n-value determination in the case of radial oscillations. In this paper we show that for β Cep stars these diagrams are only little influenced by chemical composition of elements and microturbulent velocities of stellar atmospheres.

Plots in Figs. 1–3 demonstrate the usefulness of the spectroscopic nonadiabatic observables for determination of the azimuthal order m. The domains with different m-values are very well separated between each other, especially using the observables based on the first and second moments of line profiles. The first moment measures the center-of-mass velocity, the second one – the square of the line width, and the third moment describes the skewness of the line profile. The situation is less favourable in the case of ℓ and n determination from spectroscopy, but some diagrams may still yield a useful constraint for values of these parameters.

The diagnostic diagrams presented in this paper are based on the linear nonadiabatic analysis of stellar oscillations. In analogy with photometric data discussed by Cugier et al. (1994) we introduce the name of *spectroscopic nonadiabatic observables* to denote amplitude ratios and phase difference for any pair of oscillating parameters derived from line profiles. In addition to $y(r)$ and $f(r)$

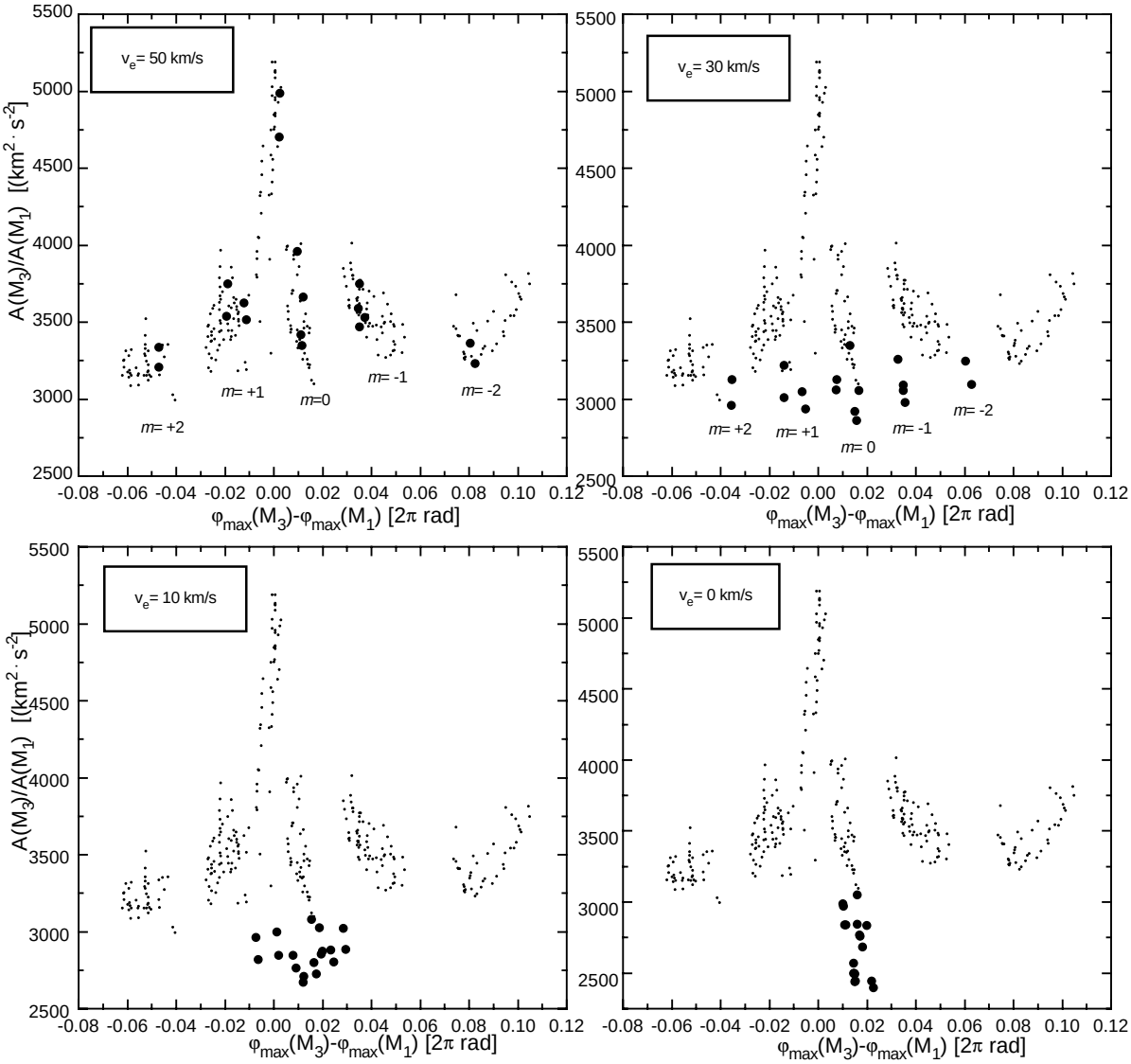

Fig. 7. As in Fig. 6, but for M_3 and M_1 measurements. For comparision we also added the data from Fig. 2 as small dots.

eigenfunctions (as in the case of photometric nonadiabatic observables) evaluation of the spectroscopic observables incorporate also the eigenfunction $z(r)$ describing variations of the horizontal displacement. A conversion of these eigenfunctions to amplitude ratios and a phase difference derived from line profiles may be directly compared with observations; one has to employ a grid of realistic models of stellar atmospheres and integrate over the stellar disk local contributions of specific intensities taking into account the Doppler effect. The spectroscopic amplitude ratios do dependent on the aspect and the azimuthal order of the mode, contrary to the photometric quantities. They also depend on the equatorial velocity of stellar rotation.

We showed that employment of the first and the second moments of line profiles are exceptionally revealing for identification of the m-value. The model points corresponding to various azimuthal orders occur in well-separated domains and there is no ambiguity in assigning the m-value to the observed modes as far as $v_{\rm e} > 20$ km s^{-1}. It should be noted, however, that the diagrams studied here are the best tools for determining the m-values if $v_{\rm e}$ is known. If we do not know $v_{\rm e}$, which is almost always the case, these diagrams are still attractive when a few components of the multiplet are observed. As mentioned above, different nonradial multiplets may have very close frequences owing to the mixed character of the modes and the spectroscopic diagrams offer an independent test for m-values in addition to the frequency measurements.

On the other hand, having already identified n, ℓ, m-values of observed modes, our diagrams offer determination of the surface value of $v_{\rm e}$, which can be compared with the stellar rotation rate derived from the rotational splitting of frequences. Rotation modifies the stellar structure, changes physical condition for wave propagation and thereby the frequencies of modes. In principle it can be possible to study the rotation rate as a function of stellar radius.

The spectroscopic diagrams discussed in this paper are complementary to the photometric data.

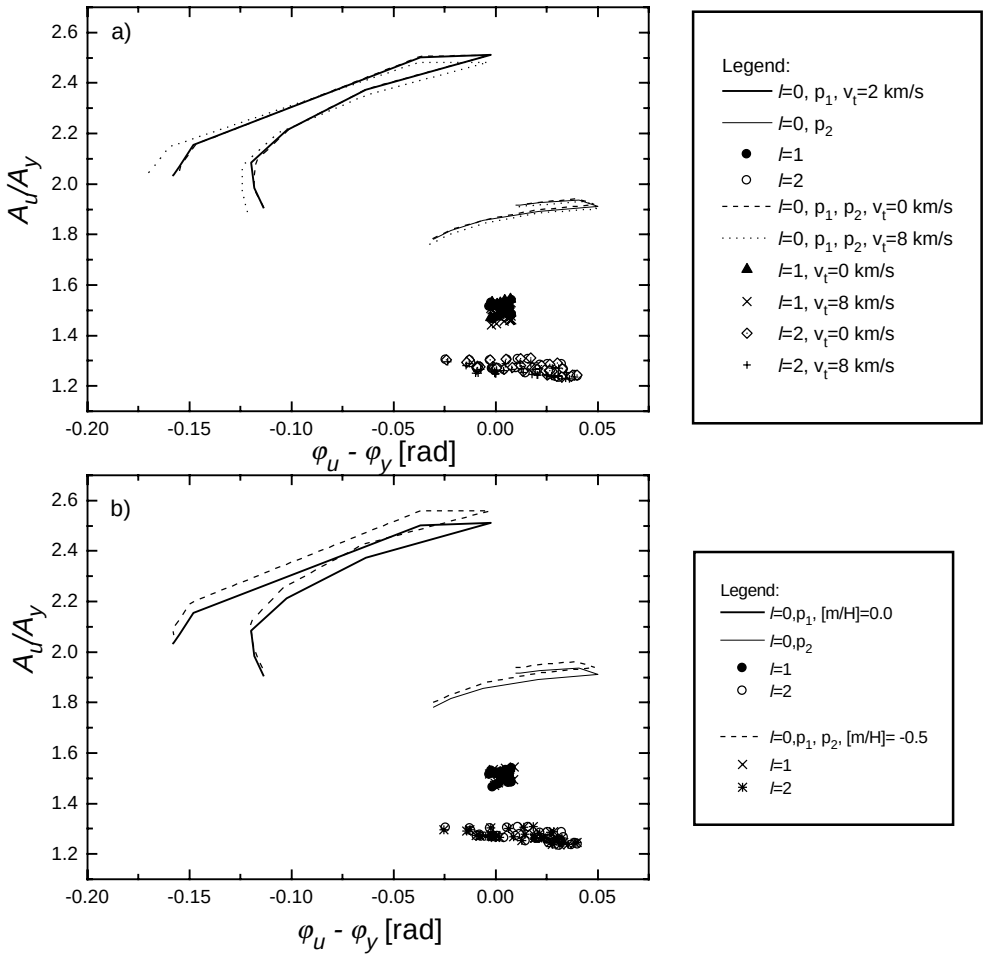

Fig. 8. The amplitude ratio vs. phase difference diagrams for the Strömgren photometric system. The data shown by different symbols correspond to unstable modes ($\ell \leq 2$) for 10 $M_\odot$ Main-Sequence models with OPAL opacities ($Z = 0.02$). The domains with different ℓ-values are well separated between each other. The upper panel also shows the effect of the microturbulent velocity ($v_\mathrm{t} = 0, 2$ and 8 $\mathrm{km\,s^{-1}}$). The lower panel shows the effect of the metallicity in the stellar atmospheres ($[m/\mathrm{H}] = 0.0$ and -0.5).

In addition to precise frequency measurements, both the photometric and spectroscopic nonadiabatic observables should be regarded as important data for asteroseismology. Determination of m-value requires high-quality spectroscopic data and the observables discussed in this paper are usually by-products of periodogram analyses of time series of observed line profiles.

Acknowledgements. This work was supported by the research grant No. 2041/W/IA/2001 from the Wrocław University.

References

Aerts, C., de Pauw, M., & Waelkens, C. 1992, A&A, 266, 294
Balona, L. A. 1986a, MNRAS, 219, 111
Balona, L. A. 1986b, MNRAS, 220, 647
Balona, L. A. 1987, MNRAS, 224, 41
Cugier, H. 1993, Acta Astron., 43, 27
Cugier, H., Dziembowski, W. A., & Pamyatnykh, A. A. 1994, A&A, 291, 143
Daszyńska, J., & Cugier, H. 1998, Astronomical Data Analysis Software and System VII, ed. R. Albrecht, R. N. Hook, & H. A. Bushouse, ASP Conf. Ser., 145, 11
Duval, P., & Karp, A. H. 1978, ApJ, 222, 220
Dziembowski, W. A., & Pamyatnykh, A. A. 1993, MNRAS, 262, 204
Gautschy, A., & Saio, H. 1993, MNRAS, 262, 213
Heynderickx, D., Wealkens, C., & Smeyers, P. 1994, A&AS, 105, 447
Kurucz, R. L. 1996, CD-ROM Nos. 13 and 19
Ledoux, P. 1951, ApJ, 114, 373
Sterken, C., & Jerzykiewicz, M. 1993, Space Sci. Rev., 62, 95
Wade, R. A., & Ruciński, S. M. 1985, A&AS, 60, 471
van Hoof, A., & Deurinck, R. 1952, ApJ, 115, 166